

Precise Determination of Nuclear Reaction Energies and Measurements of Resonance Widths

R. O. BONDELID AND C. A. KENNEDY

Nucleonics Division, United States Naval Research Laboratory, Washington, D. C.

(Received February 13, 1959)

An electrostatic analyzer with a radius of curvature of 2 meters and a deflection angle of 90° has been constructed and evaluated. It is used to provide an ion beam whose energy is precisely known and highly resolved. The absolute energy calibration is believed to be accurate to $\pm 0.05\%$, and the inherent energy resolution is 0.01% per 0.010 in. of input slit separation. Proton bombarding energies have been determined for (p,γ) reactions on F^{19} at 340.5 ± 0.3 kev, 483.6 ± 0.3 kev, 872.4 ± 0.4 kev; Al^{27} at 992.4 ± 0.5 kev; Ni^{68} at 1424.1 ± 0.7 kev, 1843.7 ± 0.9 kev; and C^{13} at 1747.6 ± 0.9 kev. Resonance widths have been measured for these reactions. They are 2.4 ± 0.3 kev, 0.9 ± 0.1 kev, 4.5 ± 0.3 kev, 100 ± 50 ev, 50 ± 50 ev, 100 ± 50 ev, and 75 ± 50 ev, respectively. The (p,n) thresholds have been determined for Li^7 at 1881.2 ± 0.9 kev and C^{13} at 3237.2 ± 1.6 kev.

I. INTRODUCTION

THE two-meter electrostatic analyzer is an instrument which is used in conjunction with the NRL positive-ion 5-Mv Van de Graaff electrostatic accelerator.¹ This analyzer provides a method of measuring the energy of the ion beam from the Van de Graaff and a method of sharply limiting the energy spread of the beam. The first of these functions is achieved by measuring the geometry of the analyzer and the voltage applied to the deflecting plates of the analyzer; the second function is achieved by utilizing the direction and velocity focusing properties of the electrostatic field.

Early applications of electrostatic analyzers were in the field of mass spectroscopy. The concurrent developments in the nonrelativistic theory for the focusing of charged particles by an electrostatic field formed by a cylindrical condenser were due to Hughes and Rojansky,² Dempster,³ and Herzog.⁴ Herzog developed the general theory for the nonrelativistic focusing of charged particles by crossed electric and magnetic fields and then applied the equations to the special cases of pure electric or magnetic fields. Later, Millet⁵ considered the relativistic focusing of charged particles by crossed electric and magnetic fields for the special case where the object and image are within the field.

Several cylindrical analyzers have been constructed especially for use with Van de Graaff accelerators. Herb, Snowden, and Sala⁶ give a rather comprehensive treatment of the corrections and errors that should be taken into account when using the instrument for absolute determination of beam energy. Honnold and Miller⁷ have developed a relativistic theory for the focusing of

charged particles through a cylindrical electrostatic analyzer for the general case when the object and image are outside of the field. The fringing electric field effects have been treated by Herzog,⁴ Herb *et al.*,⁶ Allison *et al.*,⁸ and Monahan.⁹

II. DESIGN AND CONSTRUCTION

Voltages of equal magnitude but of opposite sign are applied to the two plates of the NRL two-meter cylindrical electrostatic analyzer. This means that the geometric mean radius is at zero potential. A particle entering the analyzer at this point experiences no linear acceleration due to the presence of the deflecting field. The orbit of this particle is called the mean-line orbit and is used to determine the absolute calibration equation of the instrument:

$$V' = 2V_0 \frac{d}{b} (1-\gamma)(1-\mathcal{C}). \quad (1)$$

The relativistic correction term is $\gamma = eV_0/2m_0c^2$ and the internal magnetic field correction term is $\mathcal{C} = (Be r_0/c)(2em_0V_0)^{-\frac{1}{2}}$, where V' is the total voltage applied to the analyzer plates, V_0 is the particle voltage as determined by the Van de Graaff, d is the plate separation, b is the arithmetic mean radius, e is the charge on the particle, m_0 is the particle rest mass, c is the velocity of light, B is the vertical component of the magnetic field in the region between the plates, and r_0 is the geometric mean radius. Gaussian units are used. The quantities (d/b) , γ , and \mathcal{C} are approximations but contribute errors the order of 1 part in 10^6 , as discussed by Herb *et al.*⁶ Corrections to be applied to the results obtained by use of this expression are discussed in the section on errors. If the correction factors are ignored, then the equation is simply

$$V' = V_0(2d/b).$$

¹ Dunning, Bondelid, Fagg, Kennedy, and Wolicki, report of Naval Research Laboratory progress, May, 1955. A detailed discussion of the two-meter electrostatic analyzer is contained in Naval Research Laboratory Report NRL-5083 (unpublished).

² A. L. Hughes and V. Rojansky, *Phys. Rev.* **34**, 284 (1929).

³ A. J. Dempster, *Phys. Rev.* **51**, 67 (1937).

⁴ R. Herzog, *Z. Physik* **89**, 447 (1934).

⁵ E. Millet, *Phys. Rev.* **74**, 1058 (1948).

⁶ Herb, Snowden, and Sala, *Phys. Rev.* **75**, 246 (1949).

⁷ V. R. Honnold and W. C. Miller, Technical Report No. 2, University of Notre Dame, 1953 (unpublished).

⁸ Allison, Frankel, Hall, Montague, Morrish, and Warshaw, *Rev. Sci. Instr.* **20**, 735 (1949).

⁹ J. E. Monahan, *J. Appl. Phys.* **24**, 434 (1953).

From this it can be seen that if the maximum voltage of the particle to be deflected is 5 million volts and the voltage applied to the deflecting plates of the analyzer is 50 kv, then the ratio $b/2d$ must be approximately 100. The parameter d , the plate separation, has been chosen to be 1 centimeter to provide good high-voltage characteristics and to reduce the percentage error in the measurement of this distance (d can be measured to an accuracy of ± 0.0001 inch, i.e., $\pm 0.025\%$). Thus b , the arithmetical mean radius of the instrument, must be 2 meters. The deflection angle was chosen to be 90° for convenience in fabrication, installation, and use of the analyzer.

The object and image distances are chosen after consideration of the equation for focusing of ion paths^{4,7}:

$$(l' - g)(l'' - g) = f^2, \quad (2)$$

where $f = (r_0/k) \csc k\Phi$, $g = (r_0/k) \cot k\Phi$, $k = \sqrt{2}$, and Φ is the total analyzer angle. The quantity l' is the object distance, measured from the object to the electrical end of the analyzer at the input. The quantity l'' is the image distance and is measured from the image point to the electrical end of the analyzer at the output. Choice of either one of these quantities fixes the other. The quantity l'' was chosen using the following consideration: The electrical end of the deflection plates is made to coincide with the geometrical end by using properly placed shields. The problem of placing these shields is the "bend in a Leyden jar" problem with corrections applied for finite opening between the shields and for rounding of the ends of the plates.^{4,6,9} The electrical shields at the output are used to form the image distance l'' . In the case of the present analyzer this image distance is approximately $\frac{1}{8}$ inch. The object distance l' is then about 72.8 inches. Electrical shields are placed $\frac{1}{8}$ inch from the geometrical ends of the deflecting plates at the input to the analyzer and are used as the collimating or limiting aperture.

The slits forming the input aperture (object) are mounted on a stand which is securely bolted to the floor. Each slit is adjustable by means of a micrometer head screw which is enclosed in the vacuum.

The deflection plates of the electrostatic analyzer, made from type 303 stainless steel, were rolled from a straight section 2 inches by 4 inches in cross section and machined to the final dimension, $1\frac{1}{2}$ inches high by 3 inches wide. The separation between the plates is about 0.4 inch. Spring-out occurred during machining due to relief of rolling stresses. When the springout leveled off, the plates were considered ready for the final machining operation. The plates are mounted on a stainless steel base plate which in turn is mounted on 25 6-inch square pads in a 5 by 5 matrix on an H -beam framework. The base plate is bolted loosely at each pad so that it is free to slide on the pads during changing temperature conditions. Supporting the deflection plates are Microy insu-

lators $1\frac{1}{2}$ inches thick to each side of which are bonded stainless steel disks. The bottom disk is then securely fastened to the base plate and the deflection plate is fastened to the top disk. There are 7 insulators supporting each plate. Final machining of each deflection plate was done in position.

The deflection plates are covered by a brass box. The vacuum seal is obtained by use of a round rubber gasket. The vacuum within the analyzer is maintained by a 4-inch diffusion pump on top of which is mounted a liquid nitrogen trap. A 4-inch line between the analyzer box and the trap is constructed in a manner such that there is no optical path between the cold surface of the trap and the deflection plates of the analyzer.

A radius arm whose center of swing is located at the center of the radius of curvature of the analyzer plates holds an air gauge which is used to measure the variation in radius of the plates and to measure the separation, d , between the plates. A high-precision Timken class O bearing is used to maintain the center of swing of the arm. The air gauge is calibrated with gauge blocks. Figure 1 shows the plate separation as a function of angle at various gauge positions measured from the top of the plates. Over the region from the center of the plates to $\frac{1}{4}$ inch above the center of the plates the variation of gap is ± 0.0002 inch. Because of this relative uniformity of gap spacing, the charged particle beam is brought through the analyzer in this region. The horizontal component of the electrical field over this region varies from 0.01% to 0.001% of the total electrical field. No correction is made in the final data for this variation. Herb *et al.*⁶ have shown that the average gap, d , can be determined from the contour data using the expression

$$d = \frac{\sqrt{2}}{1 - \cos\sqrt{2}\Phi} \int_0^\Phi D(\theta) \sin[\sqrt{2}(\Phi - \theta)] d\theta, \quad (3)$$

where $D(\theta)$ is the separation at angle θ .

Various known points have been established on the base plate. By using these points and gauge blocks, it is possible to determine the radius of curvature of the plates and the angle of deflection. The arithmetical mean radius, b , is 78.7468 ± 0.002 inches and the analyzer angle Φ is 90.00 ± 0.02 degrees.

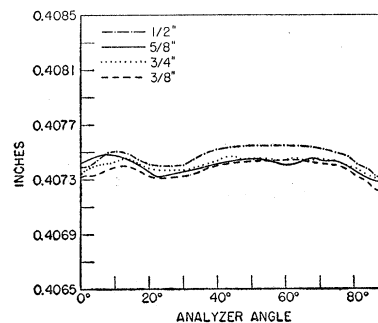


FIG. 1. Variation in gap over the face of the plates as a function of depth.

III. ENERGY RESOLUTION

An ion that enters the analyzer at a position l' from the deflection plates and displaced a distance b' from the mean line orbit leaves the analyzer at a distance l'' from the deflection plates and displaced a distance b'' given by the expression⁴

$$b'' = (\epsilon/2)(1-M)r_0 + b'M, \quad (4)$$

where ϵ is the fractional deviation of the energy of the ion from the mean-line orbit energy, and M is the magnification given by $M = -(l''-g)/f$. For the two-meter analyzer, M is -0.6 .

It is convenient to think of the quantity b' as having limiting values to either side of the mean-line orbit, i.e., an aperture is placed at l' having a width $2|b_{\max}'|$. A plot of b' vs b'' with ϵ taking on values from 0 to $\pm \epsilon_{\max}$ will show that in the general case for a uniform distribution of energies at l' the output distribution will take on the form of a truncated triangle, and in the special case where $b_{\max}'' = b_{\max}'M$ the form of the output distribution is an isosceles triangle.

If now apertures are placed at l' and l'' of total width w' and w'' , and w'' is set equal to $w'|M|$, then Eq. (4) can be written (since M is inherently negative)

$$w'' = \epsilon_{\max}(1-M)r_0 - w'. \quad (5)$$

Since ϵ_{\max} refers to $\frac{1}{2}$ the total fractional energy spread, then Eq. (5) written in terms of ϵ_{tot} becomes

$$\epsilon_{\text{tot}} = 4w''/(1-M)r_0,$$

where ϵ_{tot} represents the base of the energy distribution isosceles triangle. Resolution is commonly quoted as the full width at half maximum of a distribution curve. Using this criterion, the above equation shows that the energy resolution of the two meter electrostatic analyzer is 0.01% per 0.010 inch of input aperture opening.

IV. MAGNETIC FIELD CORRECTIONS

The earth's magnetic field induces a magnetic field in the analyzer. To a first approximation only the vertical component of the field is effective in deflecting the ion beam. The component within the analyzer acts to deflect the beam in the same direction as the electric field. Since the correction to the energy introduced by the magnetic field is small it can be treated as uniform over the region of deflection. The internal magnetic field as a function of analyzer angle is shown in Fig. 2. Equation (1) contains the correction for the magnetic field within the analyzer.

The magnetic field along the distance l' causes an energy correction to be necessary because it effectively changes the direction of entry of the ion beam, which in effect shifts the source slightly off axis. The correction for this, given by Herb *et al.*,⁶ is

$$\mathcal{E}_{\text{ext}} = \frac{l'}{1-M} \left(\frac{l'M}{r_0} - \frac{\partial M}{\partial \phi} \right) \frac{1}{r_B}, \quad (6)$$

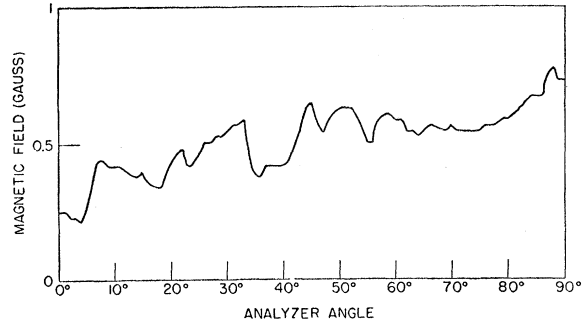


FIG. 2. The internal magnetic field.

where $r_B = c(2meV_0)^{1/2}/eB_{\text{ext}}$ and M is the magnification. Because l' is so small, the effect of the magnetic field here is neglected. The magnetic field between the plates is measured by a device that makes use of the effect of a magnetic bias on a core of ferromagnetic material that is driven to partial saturation by a sinusoidal voltage.^{10,11} If there is no magnetic bias on the core, only odd harmonics of the fundamental will be present. If the core material is biased as it would be in the earth's field, even harmonic components of current will be present. The second harmonic component can then be used as a measure of the magnetic field in which the material is placed.

V. ELECTROSTATIC ANALYZER POWER SUPPLY

The electrostatic analyzer requires a stable source of potential for the plates. Since the current drain is very low, batteries or a rectifier-filter type of regulated power supply could be used.¹² Batteries were not considered acceptable because of their bulk, temperature coefficient, and difficulty of getting continuous voltage control.

A rectifier-filter type of power supply, having continuous voltage adjustment and adequate regulation, can be made. The following discussion gives the requirements of the power supply, a description of the design, and evaluation of the power supply.

A. Requirements

To meet the design requirements of the electrostatic analyzer, the power supply must provide simultaneously equal positive and negative voltages up to a maximum total potential of 70 kv. The voltage should be continuously adjustable from zero, preferably in several overlapping ranges. Voltage stability over the range of about 7 kv to 70 kv should be better than 0.01% of the operating voltage for periods of several hours, and some means of monitoring the potential should be available. The error in voltage measurement should be less than 0.03%. Ripple voltage at the plates for all normal

¹⁰ Bhattacharjee, Waldman, and Miller, *Phys. Rev.* **95**, 404 (1954).

¹¹ Adams, Dressel, and Towsley, *Rev. Sci. Instr.* **21**, 69 (1950).

¹² R. L. Henkel and B. Petrie, *Rev. Sci. Instr.* **20**, 729 (1949).

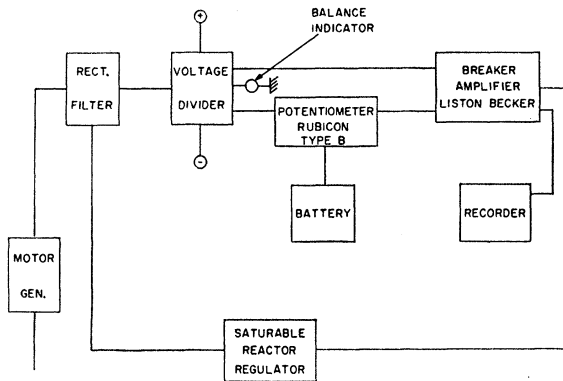


FIG. 3. Block diagram of electrostatic analyzer power supply.

operating conditions should be less than 0.01% of the operating voltage. Inequality of the positive and negative output voltages should be less than 0.3%.

B. General Circuit Description

A block diagram of the power supply system is shown in Fig. 3. A 400-cycle permanent-magnet generator driven by an induction motor is used to supply the primary power for the high-voltage rectifier system. This motor-generator combination provides a relatively stable primary voltage at the constant load used since it is fairly insensitive to normal 60-cycle line voltage changes. Normal frequency changes do not constitute a problem.

The rectifier system is a conventional full-wave voltage-doubler system in which the mid-voltage point is grounded, thereby supplying equal positive and negative potentials at the output terminals. A capacity filter, having sufficient capacity to give a ripple below 0.01% for normal loads, is used.

The precision voltage divider is made up of 68 one-megohm wire-wound resistors arranged in two spiral columns. Between each group of 3 resistors, there is a gradient disk to provide a uniform gradient down the column and minimize the possibility of corona discharge. At the ground end of each of the two columns, there is a series of resistors having a total resistance of 1 megohm, with taps at 750 ohms, 1500 ohms, and 2250 ohms for each of the three voltage ranges. This makes a total resistance of 70 megohms, 35 megohms in each column. The high-resistance units are made with Evanohm which has a temperature coefficient of resistance of 20 parts per million per °C, and a thermal emf to copper of 2 microvolts per °C. The low-resistance units are wound of Manganin which has a temperature coefficient of resistance of 15 parts per million per °C, and a thermal emf to copper of 1.5 microvolts per °C.

To minimize the effects of humidity, all the resistor elements are encapsulated and the entire divider assembly is housed in a sealed enclosure. A fan and thermostatically controlled heater are also included to

minimize the effect of ambient temperature change, and the effect of divider dissipation changes with voltage.

The voltage reference system is composed of a Rubicon type "B" potentiometer, a standard cell, and a low-discharge type storage cell. Since the potentiometer was designed for operation from either a 3- or 6-volt source, some of the auxiliary resistors have been changed to make operation from a 2-volt cell possible. The potentiometer was also remounted for rack and panel-type construction, and the back was enclosed in a Lucite case large enough to contain the standard cell. The Lucite enclosure is thick enough to serve as a thermal shield to minimize the effect of rapid changes in ambient temperature on both the standard cell and the potentiometer. The storage cell, a Willard Type *DD5-1*, 200-ampere-hour cell, is enclosed in a Lucite box having an additional thermal-insulating liner. A temperature compensating resistance of copper wire, series connected, is wrapped around the battery.¹³ The storage-cell temperature coefficient is plus 410 microvolts per °C. For the 11-ma load current required by the potentiometer, the required copper wire resistance is 9.55 ohms. The insulating box is not intended to maintain the battery at constant temperature, but rather to cause the temperature to change slowly enough for the battery and compensating resistance to change in equilibrium.

The difference between the potentiometer output voltage and the voltage on the appropriate tap of the precision voltage divider constitutes the error voltage. This error voltage is fed to a Liston Becker type 10-A, dc Breaker Amplifier. The amplifier output is fed to the regulator, as well as two error indicators—one a panel meter, and the other a 1-ma Esterline-Angus recorder. The recorder provides a continuous record of voltage deviations from the reference value.

The regulator consists of a saturable reactor connected in series with the primary of the high-voltage transformer. The impedance of the reactor is varied in accordance with the error signal, which is applied to the grid of the control tube in the dc circuit of the reactor.

C. Problems

The high-voltage transformer secondary had an inductance high enough that it was self-resonant below the 400-cycle operating frequency. This caused the input impedance as seen at the transformer primary to be highly capacitive. The transformer current due to total circuit capacity loading exceeded the ratings. To minimize capacity the filament transformer for the negative rectifier was redesigned to provide as low a capacity from the secondary to the core and primary as possible.

The proximity of 60-cycle circuits caused objectionable interference at the input of the breaker amplifier primarily due to magnetic coupling in the circuits ahead of the amplifier input terminals. To minimize this difficulty all possible leads were run as shielded twisted

¹³ F. K. Harris, National Bureau of Standards (private communication).

pairs. The low-voltage resistors in the voltage divider were arranged with the ground leads in a way such that the area of the circuit loop was a minimum. The temperature-compensating element on the potentiometer source battery was wound as a bifilar winding to reduce magnetic coupling at this point. Interference from 60 cycles that remained was further reduced by means of a low-pass filter at the amplifier input.

In the initial design, regulation was not possible over the required range of the two higher voltage tap positions. This difficulty was due to series resonance operation at the 400-cycle power-supply frequency of the transformer-saturable reactor circuit. Near the low-voltage end of each of these ranges, the impedance would swing from the inductive region through resonance to the capacitive region as the operating voltage was lowered. This phase reversal, from a lagging to a leading impedance, required a reversal of the error signal to maintain regulator operation. The problem was not encountered on the low-voltage range, because the saturable reactor inductance was sufficiently high to produce series resonance well below the power-supply frequency over the entire operating range. High-inductance operation of the saturable reactor on the higher voltage ranges was not feasible because of the limits in the source voltage. The problem was solved by shunting the transformer primary with an inductance of low enough value to produce resonance with the transformer well above 400 cycles over the entire operating voltage range. Since the load seen by the saturable reactor is now inductive, there is no resonance phenomenon and regulation is possible anywhere in the operating range.

D. Test and Evaluation

In order to evaluate the power-supply regulator, a comparison was made between the terminal voltage stability with and without the regulator in operation. Without the regulator, the voltage fluctuated about $\pm 0.75\%$ of the terminal voltage at 10 kv. With the regulator, the fluctuation from a cold start was $\pm 0.02\%$ at 10 kv, an improvement of 38 times. Typical values of short-term regulation, after warmup, range from about

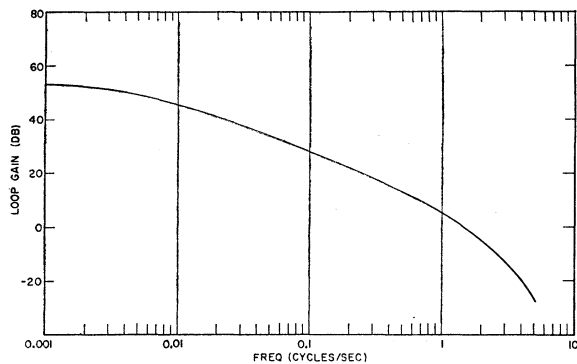


FIG. 4. Loop gain of regulator system.

TABLE I. Resistance ratios.

Tap No.	Nominal ratio (NR)	Left stack % of NR		Right stack % of NR	
		Computed	Measured	Computed	Measured
1	46 666.7	99.78	99.78	99.69	99.69
2	23 333.3	99.78	99.79	99.68	99.68
3	15 555.5	99.78	99.78	99.69	99.69

$\pm 0.003\%$ of the terminal voltage on the 25-kv range to $\pm 0.007\%$ on the 75-kv range.

The gain characteristics of the regulator loop are shown in Fig. 4. The maximum gain of about 430 occurs at dc, and falls to 1 at about 1.5 cycles. The phase shift is 360° at about 4 cycles, and with the phase shift characteristics of the system limits the maximum dc gain to about 430.

When completed, the precision voltage divider was sent to the National Bureau of Standards for calibration. This calibration was in two parts. The first consisted of measurement of the divider ratio at voltage increments from 5 kv to 35 kv on each of the two columns for all three tap positions. Measurements were made with the heaters operating normally, and with the heaters off. The maximum variation indicated is 0.02% and the limit of measurement precision was 0.01% . With the heaters operating, the air temperature within the enclosure was about 33°C , and varied about 2°C from zero voltage to maximum divider dissipation. The second set of measurements consisted of calibration of the individual resistors at room temperature in a low-voltage bridge. To compare the two calibration results, the individual values were totalled and the divider ratio computed. These ratios were compared with the average of the room temperature high-voltage measurements. Agreement (see Table I) was $\pm 0.01\%$, or better, for all three tap positions on each stack.

The source battery for the potentiometer was checked to determine voltage drift due to the continuous potentiometer load. Under this load, the voltage drops about $225 \mu\text{v}/\text{day}$, or $9.4 \mu\text{v}/\text{hour}$. The change in potentiometer calibration due to source change is then about $4.7 \times 10^{-4}\%$ per hour after potentiometer calibration against the standard cell.

The potentiometer used for voltage reference and measurement has a calibration accuracy of $\pm 0.01\%$ above the 0.3-volt tap. In normal operation, 0.5 volt is the lowest tap position used. The standard cell used for standardizing the potentiometer is the Weston unsaturated type. It is housed in the potentiometer enclosure, which serves as a thermal shield for both. This shield minimizes the chance of rapid and unequal changes in the temperature of the cell. Under these conditions, the temperature coefficient is negligible. The potentiometer standardization sensitivity is $0.269 \mu\text{v}$ per μv of change in source battery voltage. Using the error amplifier as the detector for standardization, the potentiometer can be set to within $5 \times 10^{-4}\%$ of standard cell potential.

TABLE II. Precision of measurement of electrostatic analyzer voltage.

	Limit of error (%)
Potentiometer accuracy	± 0.01
Potentiometer setting relative to standard cell	± 0.0005
Stability	± 0.005
Standard cell accuracy	± 0.005
Temperature change	± 0.005
Voltage divider	± 0.01
Zero drift in amplifier	± 0.005
Probable error in voltage	± 0.018

The precision of voltage measurement is affected by accuracy of the potentiometer, the voltage divider, and the standard cell, as well as the stability of these components. Precision is as shown in Table II, considering the errors as random.

VI. ERRORS IN ABSOLUTE CALIBRATION

Examination of the equation for the mean-line orbit, Eq. (1), shows that the errors for absolute calibration arise from the errors in the determination of V' , d , b , and B . Since this equation is based on the supposition that the orbit is the mean-line orbit, additional errors arise from the deviations from the mean-line orbit.

As concluded in the previous section, the error in the voltage determination is $\pm 0.018\%$. The radius is determined by piling gauge blocks. From the reproducibility and estimates of the gauge block error, the uncertainty in the radius is taken to be ± 0.002 inch. Since the radius is about 78 inches, the error is $\pm 0.003\%$. The gap measurement is made up of 91 readings at 4 vertical positions for a total of 364 separate measurements. The reproducibility of the average is better than 0.00005 inch even after the gauge has been removed, then reinstalled and recalibrated. The total error in the gap is taken to be ± 0.0001 inch. Since the gap is 0.4074 inch, the error is $\pm 0.025\%$. An error introduced by vacuum deformation of the base plate is included in the stated gap uncertainty. The internal magnetic field is measured to a precision of $\pm 10\%$. Since it contributes a correction of about 0.05% for a 1-Mev proton, the error is $\pm 0.005\%$.

The external magnetic field along V' , discussed in a previous section, tends to make the source appear to come from a position off the mean-line orbit at the input. This introduces a correction of about 0.014% for

TABLE III. Summary of errors in energy determination (in %).

Voltage	± 0.018
Radius	± 0.003
Gap	± 0.025
B_{int}	± 0.005
B_{ext}	± 0.001
Slits, input, output lateral position	± 0.012
Slits, relative to plates	± 0.001
Analyzer angle, Φ	± 0.012
Rms total	± 0.035

a 1-Mev proton. Since the magnetic field can be measured to $\pm 10\%$, the uncertainty is $\pm 0.0014\%$.

The lateral positioning of the slits at the plates can be done reproducibly to 0.0001 inch. The lateral positioning of the slits at the input, or source, can be done to 0.010 inch. Examination of Eq. (4) shows that an estimate of the lateral positioning error (ϵ_p) of the slits can be made. Assuming a point source and the uncertainties given above, ϵ_p is 0.01%. The effect of moving the input slits laterally by 0.100 inch was checked by observing the apparent energy shift in a strong resonance in the $Al^{27}(p,\gamma)Si^{28}$ reaction. The data substantiated the above calculation. That a lateral positioning error of several thousandths of an inch in the limiting aperture at the input to the plates is negligible was checked experimentally by looking for an apparent energy shift in this resonance.

The distance of the shields relative to the ends of the plates can be set to ± 0.001 inch by the use of a specially ground plate. An error here has the following effects: An error in the end correction changes the effective angle of the analyzer and at the output changes V'' . The effect of these changes on the focusing condition, Eq. (2), is small enough to be neglected. Another effect is on the condition of tangency required of the mean-line

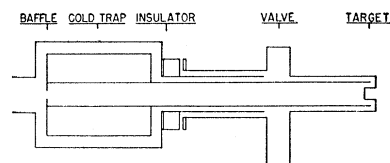


FIG. 5. The target holder.

orbit at the input to the plates. A positioning error of 0.001 inch reflects an error of about 0.001 inch at the input. The uncertainty is then $\pm 0.001\%$.

An error in the total analyzer angle, Φ , also introduces an error in the condition of tangency of the ion beam as it enters the analyzer. Equation (4) can be used to estimate this error. Half of the error in Φ is taken to be present at the input to the analyzer. The error reflected at the input aperture is ± 0.013 inch or $\pm 0.012\%$. The errors are summarized in Table III.

VII. PRECISION ENERGY DETERMINATION OF NUCLEAR REACTIONS

One of the difficulties encountered in bombarding a target with a beam of charged particles is the buildup of a surface layer of carbon due to the presence of organic contaminants from the vacuum system. To avoid the presence of carbon on the target surface, the technique employed in the present experiment is to surround the target with a surface near liquid nitrogen temperature while the target is near room temperature.¹⁴ Since the vapor pressure of the contaminants is many orders of magnitude less at liquid nitrogen temperature than at room temperature, the effect is a rapid exchange of

¹⁴ J. W. Butler and C. R. Gossett, Phys. Rev. **108**, 1473 (1957).

TABLE IV. Summary of energy measurements.

Run	Reaction energies (kev)								
	$\text{Al}^{27}(p,\gamma)\text{Si}^{28}$	$\text{C}^{13}(p,\gamma)\text{N}^{14}$	$\text{Li}^7(p,n)\text{Be}^7$	$\text{C}^{13}(p,n)\text{N}^{13}$	$\text{Ni}^{58}(p,\gamma)\text{Cu}^{59}$	$\text{Ni}^{58}(p,\gamma)\text{Cu}^{59}$	$\text{F}^{19}(p,\alpha\gamma)\text{O}^{16}$	$\text{F}^{19}(p,\alpha\gamma)\text{O}^{16}$	$\text{F}^{19}(p,\alpha\gamma)\text{O}^{16}$
1	992.3		1880.9						
2	992.3								
3	992.4	1747.6		3237.1					
4				3236.9					
5	992.4	1747.6	1881.5	3237.5					
6					1424.1	1843.7			
7	992.4						340.5	483.6	872.4
Av	992.4 ± 0.5	1747.6 ± 0.9	1881.2 ± 0.9	3237.2 ± 1.6	1424.1 ± 0.7	1843.7 ± 0.9	340.5 ± 0.3	483.6 ± 0.3	872.4 ± 0.4

contaminants from the target face to the cold surface. A target can be bombarded for several days in this arrangement and show no effects attributable to carbon build-up. The target holder (Fig. 5) has the added feature that it is possible either to change targets without exposing the cold surfaces to air, or to install a target without exposing it to air.

The present experiments have been confined to reactions producing γ rays or neutrons. The γ rays are detected with a NaI:Tl scintillator mounted on a photomultiplier tube. The neutrons are detected with a BF_3 proportional counter surrounded by a small amount of paraffin. A counter of this type is more sensitive to threshold or "slow" neutrons (1 to 100 kev) than to "fast" neutrons (above 100 kev).¹⁵ The electronics is the same for both counters. The pulses are amplified and fed into an integral pulse-height discriminator, the output of which is recorded on a scaler.

Prior to the start of an experiment using the electrostatic analyzer, the vacuum cover is removed and the interior, including the plates, is cleaned. The gap, d , is gauged according to the method described previously, the slit zeroes are determined, and the input tangential alignment is checked. The target and limiting baffle (Fig. 5) are aligned so that the beam must emerge from the electrostatic analyzer plates in the proper region, from the center to $\frac{1}{4}$ inch above the center of the plates. The cover is then replaced and the system is evacuated. After a series of measurements, the gap is again measured.

A. Strong Resonance in the $\text{Al}^{27}(p,\gamma)\text{Si}^{28}$ Reaction

Herb *et al.*⁶ have determined the proton bombarding energy at a strong resonance in the $\text{Al}^{27}(p,\gamma)\text{Si}^{28}$ reaction to be 993.3 ± 1.0 kev. This resonance is known to have a very narrow full width at half maximum. Because it is strong and narrow, it is an excellent calibration point and also provides an indication of the resolution of magnetic and electrostatic analyzers.

A series of observations were made on this resonance to determine the operational behavior of the NRL electrostatic analyzer. These are the following:

1. Measurement of absolute energy of bombarding protons: Targets of aluminum were prepared by evapo-

rating aluminum onto vacuum-heated cleaned disks of tantalum. The aluminum was approximately 5 to 10 kev thick to a 1-Mev proton beam, a thick target for this resonance. The potentiometer reading corresponding to the center point of the thick-target yield curve rise is used to compute the bombarding energy of the protons, Eq. (1). A typical yield curve is shown in Fig. 6. Several times during the period covered by the calibration runs, changes were made in the resistor stack. Since each resistor in the stack was calibrated absolutely, it was possible to change resistors and then recalculate the divider ratio. By the end of the last run, 8 resistors had been changed. The stack ratio was recalibrated by the High Voltage Laboratory at the Bureau of Standards. This result agreed to within 0.01% of the value based on the absolute resistor calibration data. The results of several runs on this resonance are presented in Table IV. The average of these runs is 992.4 ± 0.5 kev. This is to be compared with the results of Herb *et al.*⁶ (993.3 ± 1.0 kev) and Bumiller *et al.*¹⁶ (990.8 ± 0.2 kev).

2. By taking small intervals over the resonance, it appears that short-time stability of the high-voltage supply is of the order of 0.002%.

3. There was a long-time daily drift upward of the order of 0.02% in the potentiometer reading corresponding to the peak of the resonance. On successive

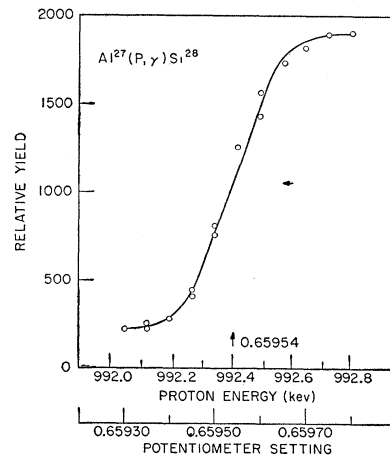


FIG. 6. The $\text{Al}^{27}(p,\gamma)\text{Si}^{28}$ yield curve of the 992.4-kev resonance.

¹⁶ Bumiller, Staub, and Weaver, *Helv. Phys. Acta* **29**, 83 (1956); Bumiller, Müller, and Staub, *Helv. Phys. Acta* **29**, 234 (1956).

¹⁵ Butler, Dunning, and Bondelid, *Phys. Rev.* **106**, 1225 (1957).

TABLE V. Comparison of present absolute measurements with previous work.^a

Reaction	NRL	Hunt ^b	Bumiller ^c	Herb ^d	Other investigators
$F^{19}(p,\alpha\gamma)O^{16}$	340.5±0.3	340.4±0.4	340.5±0.3		340.4±0.4, ^e 340.0±2.0 (rel. to 873.5) ^f
$F^{19}(p,\alpha\gamma)O^{16}$	483.6±0.3	483.1±0.5			
$F^{19}(p,\alpha\gamma)O^{16}$	872.4±0.4		871.3±0.4	873.5±0.9	872.5±1.8 ^g
$Al^{27}(p,\gamma)Si^{28}$	992.4±0.5		990.8±0.2	993.3±1.0	
$Ni^{58}(p,\gamma)Cu^{59}$	1424.1±0.7				
$Ni^{58}(p,\gamma)Cu^{59}$	1843.7±0.9				
$C^{13}(p,\gamma)N^{14}$	1747.6±0.9				1746.9±0.8, ^h 1747.6 ⁱ
$Li^7(p,n)Be^7$	1881.2±0.9			1882.2±1.9	1881.3±0.7, ^j 1881.4±1.1, ^k 1879.7±1.1 ^k 1881.2±1.9 ^l
$C^{13}(p,n)N^{13}$	3237.2±1.6				3236.0±3.0 ^m 3238.0±4.0 ⁿ

^a All energies are in kev.^b See reference 28.^c See reference 16.^d See reference 6.^e See reference 26.^f See reference 27.^g See reference 29.^h See reference 22.ⁱ See reference 23.^j See reference 19.^k See reference 18.^l See reference 20.^m See reference 24.ⁿ See reference 25.

mornings the reading was the same. This drift disappeared when the analyzer was operated with the high-wattage overhead lights turned off. In connection with this drift, other possible thermal effects were investigated and eliminated.

4. Changes in slit settings produced a shift in the potentiometer readings which substantiated the calculations made previously.

5. Periods of long bombardment (several hours) produced no change in the potentiometer reading corresponding to the peak of the resonance, indicating that there was no appreciable buildup of carbon on the face of the target. A surface layer corresponding to 50-ev change in beam energy could have been observed easily.

6. Instrument resolution: For a very narrow resonance, and small contributions from Doppler broadening, power supply ripple and regulation, the shape of the thick-target yield curve is determined by the distribution of energies in the beam out of the electrostatic analyzer. The preceding statement will hold true for a thin-target yield curve if the thin target has a thickness which is much less than the spread in energies out of the

electrostatic analyzer. The 992.4-kev resonance in the $Al^{27}(p,\gamma)Si^{28}$ reaction was examined with an input aperture of 0.060 inch and a thick target, and an input aperture of 0.050 inch and a very thin target. Under these conditions, the base of the isosceles distribution triangle is 0.12% and 0.10% of the nominal energy, respectively, or for this resonance 1.2 kev and 1.0 kev, respectively. The resonance width, the Doppler broadening, and the power supply regulation represent a spread in energy very much less than this (order of 50 to 100 volts each). The thin target was estimated to be <400 ev thick. In both the thick- and the thin-target case, the yield curve substantiated the predicted triangular distribution.

7. Linearity: Using thin targets and the mass-2 proton beam on this and other resonances, the linearity of the analyzer has been established to be within 0.02% over the energy range from 340 kev to 3 Mev.¹⁷

B. $Li^7(p,n)Be^7$ Threshold Bombarding Energy

This reaction provides a well-known calibration point, measured by several investigators.^{6,18-20}

For the present measurement, LiF was evaporated onto a tantalum backing. The front face of the target was covered with stainless steel mesh to prevent error due to charge accumulation on the nonconductive LiF. As the bombarding energy is increased, neutrons first start to appear when the higher-energy side of the incident particle group first reaches threshold. This lower-energy portion of the excitation curve will be rounded due to target thickness, Doppler shift, and energy spread of the incident beam. As the energy increases still further, the curve will appear to rise almost linearly. An extrapolation of the linear portion then provides an approximation to the true threshold.²¹ In Fig. 7 is shown the number of neutron counts as a

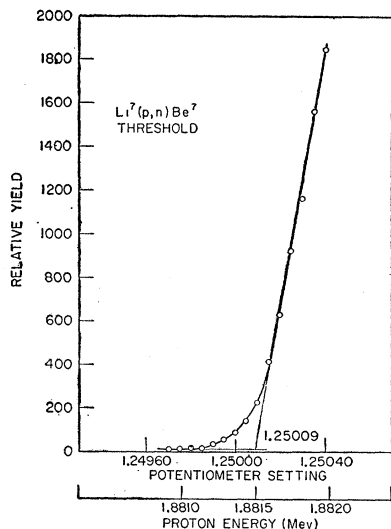


FIG. 7. The $Li^7(p,n)Be^7$ threshold yield curve.

¹⁷ Bondelid, Butler, and Kennedy, *Bull. Am. Phys. Soc.* **2**, 381 (1957).

¹⁸ Jones, Douglas, McEllistrem, and Richards, *Phys. Rev.* **94**, 947 (1954).

¹⁹ W. J. Sturm and V. Johnson, *Phys. Rev.* **83**, 542 (1951).

²⁰ Shoupp, Jennings, and Jones, *Phys. Rev.* **76**, 502 (1949).

²¹ Newson, Williamson, Jones, Gibbons, and Marshak, *Phys. Rev.* **108**, 1294 (1957).

function of the electrostatic analyzer potentiometer setting. The present result for this threshold is summarized in Table IV. The average is 1.8812 ± 0.009 Mev. Previous results^{6,18-20} are shown in Table V. The weighted average of all results is 1.8811 ± 0.0005 Mev.

The final error in the bombarding energy includes the error in the electrostatic analyzer plus estimated target and extrapolation effects.²¹ The input aperture was set for an opening of 0.030 inch.

The resistor stack of the power supply was checked by observing the potentiometer settings corresponding to this threshold on the tap 2 and tap 3 position. The agreement is better than 0.01%.

C. Strong Resonance in the $C^{13}(p,\gamma)N^{14}$ Reaction

A target of C^{13} was prepared by heating a strip of molybdenum in an atmosphere of C^{13} -enriched (60%) CH_3I . The resulting target was approximately 5 kev thick to a 1.75-Mev proton beam. A strong resonance in the region of 1.75 Mev was examined using input apertures of 0.010 inch and 0.030 inch. Figure 8 shows the

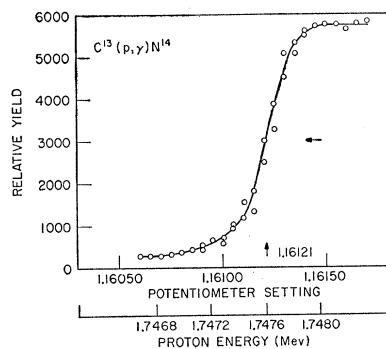


FIG. 8. The $C^{13}(p,\gamma)N^{14}$ yield curve at 1.7476 Mev.

γ -ray yield as a function of potentiometer setting for an input aperture of 0.010 inch. The middle of the rise of the yield curve is taken to be the peak of the resonance. There may be some doubt about the validity of this choice because of the asymmetrical shape of the curve. This shape could be caused by nonuniform target composition. It is to be noted that the error this introduces in the choice of the resonance peak is of the order of the half-width of the resonance, about 0.01%. The average proton bombarding energy, as determined from two runs on the same target, is 1.7476 ± 0.0009 Mev (see Table IV). Marion and Hagedorn²² report 1.7469 ± 0.0008 Mev relative to the $Li^7(p,n)Be^7$ threshold at

²² J. B. Marion and F. B. Hagedorn, Phys. Rev. **104**, 1028 (1956).

²³ R. M. Williamson and W. Haeberli, quoted by Marion and Hagedorn, reference 22.

²⁴ Richards, Smith, and Browne, Phys. Rev. **80**, 524 (1950).

²⁵ R. A. Chapman and H. Bichsel (unpublished results), quoted by J. B. Marion and T. W. Bonner (unpublished report).

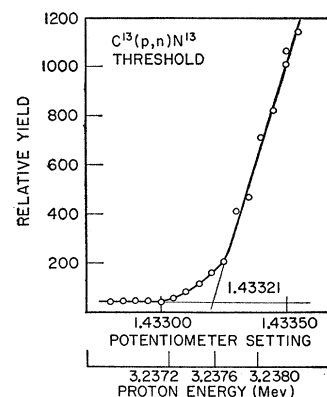
²⁶ A. H. Morrish, Phys. Rev. **76**, 1651 (1949).

²⁷ A. Fowler and C. C. Lauritsen, Phys. Rev. **76**, 314 (1949).

²⁸ S. E. Hunt, Proc. Phys. Soc. (London) **A65**, 982 (1952).

²⁹ K. F. Famularo and G. C. Phillips, Phys. Rev. **91**, 1195 (1953).

FIG. 9. The $C^{13}(p,n)N^{13}$ threshold yield curve.



1.8811 ± 0.0005 Mev. Williamson and Haeberli²³ give 1.7476 relative to the same calibration.

D. $C^{13}(p,n)N^{13}$ Threshold Bombarding Energy

A typical neutron yield curve is shown in Fig. 9. Table IV summarizes the results of the observations on this threshold. The average threshold bombarding energy is 3.2372 ± 0.0016 Mev. Richards *et al.*²⁴ measured this threshold relative to the $Li^7(p,n)Be^7$ threshold using targets of normal carbon which contains 1.1% C^{13} . They quote 3.236 ± 0.003 when normalized to 1.882 Mev for the $Li^7(p,n)Be^7$ threshold. Chapman and Bichsel²⁵ report 3.238 ± 0.004 relative to several reactions.

An input aperture setting of 0.030 inch was used for this measurement.

E. Two Resonances in the $Ni^{58}(p,\gamma)Cu^{59}$ Reaction

Two resonances in this reaction were examined. A target of Ni^{58} was prepared by electrodeposition onto a silver backing. The yield curves are shown in Fig. 10.

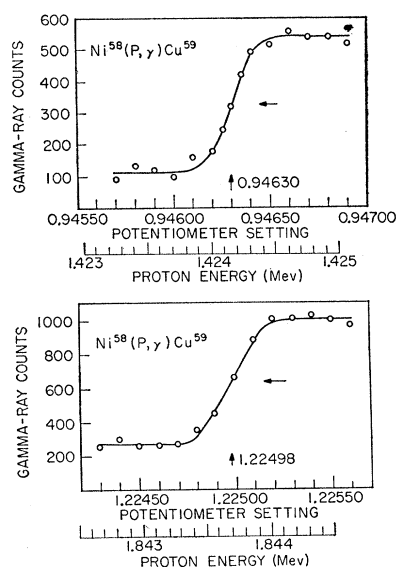


FIG. 10. The $Ni^{58}(p,\gamma)Cu^{59}$ yield curves at 1.4241 and 1.8437 Mev.

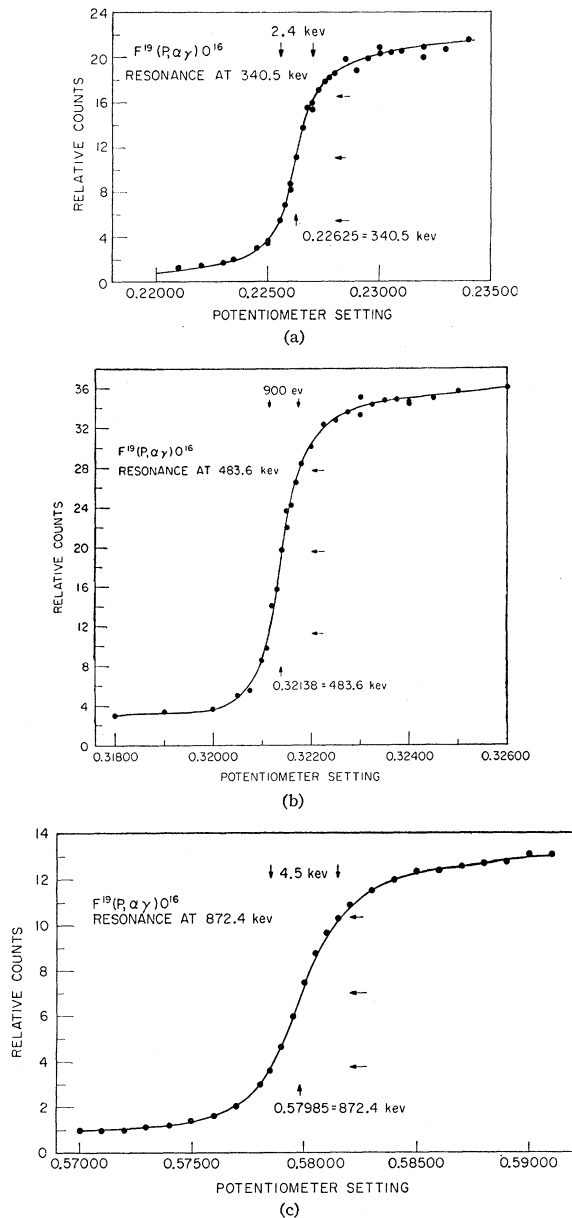


FIG. 11. The $F^{19}(p, \alpha\gamma)O^{16}$ yield curves at 340.5, 483.6, and 872.4 keV.

The results (Table IV) are 1.4241 ± 0.0007 Mev and 1.8437 ± 0.0009 Mev.¹⁴

F. Three Resonances in the $F^{19}(p, \alpha\gamma)O^{16}$ Reaction

Three resonances in this reaction were examined. A target of CaF_2 was prepared by evaporation onto a tantalum backing. The yield curves are shown in Fig. 11. The widths of the resonances, Γ , determined by the interquartile separation, are also shown in Fig. 11 and summarized in Table VII. A summary of the determination of the bombarding energies is in Table IV. They are 340.5 ± 0.3 , 483.6 ± 0.3 , and 872.4 ± 0.4 keV.

Table V summarizes all of the absolute calibration data and compares them with previous work.

VIII. MEASUREMENT OF RESONANCE WIDTH

The shape of a yield curve from a resonance is determined by the natural shape of the resonance, the factors contributing to the spread in the energy of the bombarding beam, and the thickness and composition of the target. A thin-target yield curve can give a good value for the full width at half-maximum of a resonance provided that this full width is greater than the thickness of the target and the factors contributing to energy spread of the incident particle beam. When the resonance width is the order of the thickness of the target, the analysis becomes complicated and uncertain due to the doubt in the thickness of the target and the effects of straggling. The shape of a thick-target yield curve, on the other hand, depends only on uniformity of target composition, resonance width, and incident particle energy spread. In this case, when the resonance width is large compared to the incident-beam energy spread it can be shown easily that the width of the resonance can be found from the interquartile distance on the yield curve.³⁰ When the resonance width is of the same order as the incident beam energy spread, the most satisfying method of determining the width of the resonance is to compute a family of yield curves with Γ as the parameter, and comparing with the data.

Factors which contribute to the energy spread of the beam are those which arise from the resolution of the analyzer, the modulation of the incident beam due to power supply ripple and regulation, and the Doppler broadening introduced by the thermal motion of the target nuclei.

To arrive at an expression for the contribution due to Doppler broadening, it has been assumed that the distribution of component velocities of target nuclei in the direction of the incident beam can be represented by a probability distribution. Secondly, it has been assumed that the relationship between mean square velocity and most probable velocity is the same in solids as it is in gases. Thirdly, the Debye theory has been used and it is assumed that the Debye temperature, Θ , is not very different than the target temperature T . The distribution of particle energies about the mean proton bombarding energy, E_p , due to Doppler broadening is represented by the Gaussian

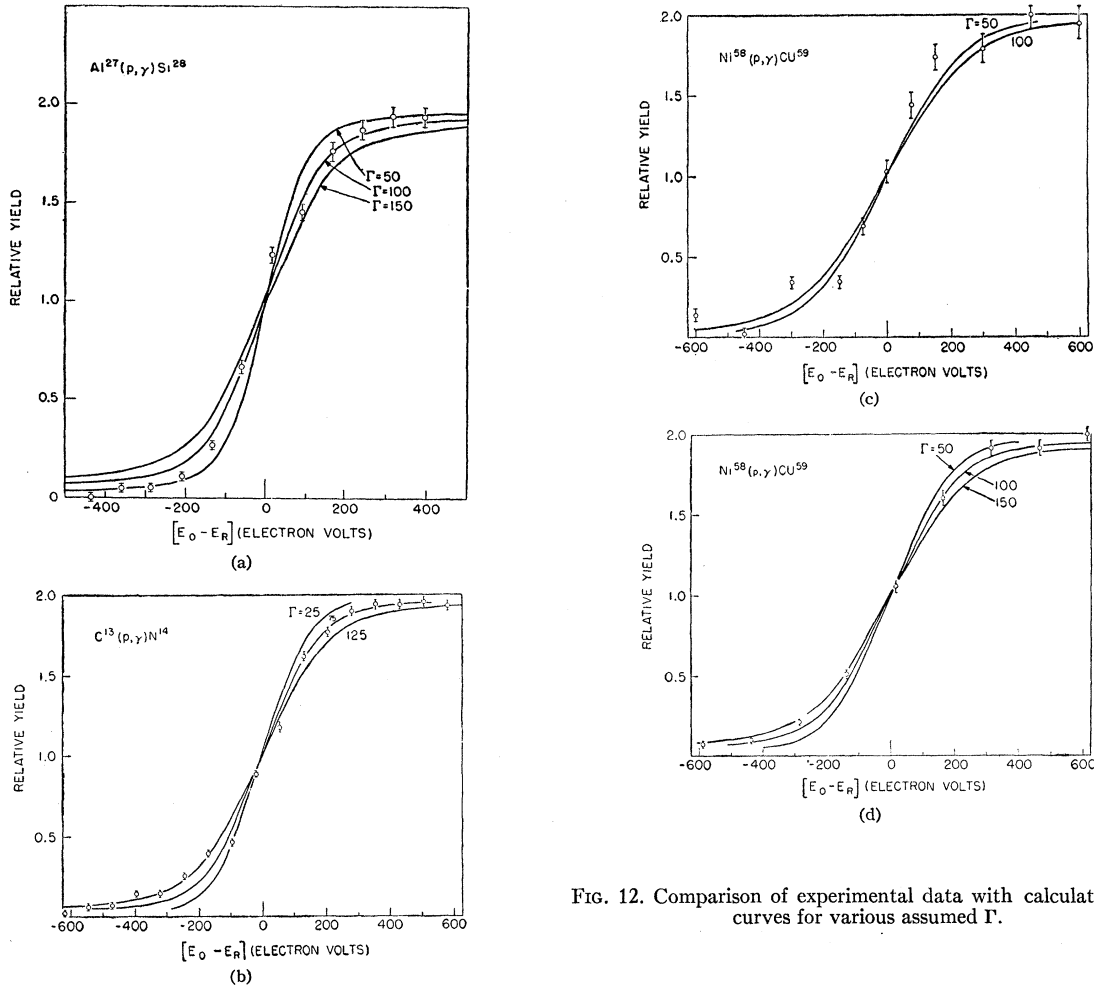
$$N(E)dE = \frac{N_0}{(2\pi)^{1/2}\Delta_3} \exp[-(E_p - E)^2/2\Delta_3^2]dE, \quad (7)$$

where

$$\Delta_3 = \left[\frac{2m}{M} E_p kT \left(1 + \frac{\Theta^2}{20T^2} \right) \right]^{1/2},$$

m is the mass of the bombarding particle, and M is the

³⁰ Fowler, Lauritsen, and Lauritsen, *Revs. Modern Phys.* **20**, 236 (1948).


 FIG. 12. Comparison of experimental data with calculated yield curves for various assumed Γ .

mass of the target nucleus. The principal difference between this expression and that found from application of the perfect gas law is the assumption that there is an equal division between potential and kinetic energy in the oscillator, i.e., the target nucleus.

To simplify the over-all problem, it is assumed that the distribution of energy in the beam due to the geometry of the analyzer and the factors involving regulation and ripple can be represented by a Gaussian. With this assumption a new Gaussian representing the distribution of energy in the beam is written where the Δ 's are defined as follows: Δ_1 describes the instrument resolution, Δ_2 describes the modulation of the beam due to the power supply ripple and regulation, Δ_3 is the Doppler broadening, and $\Delta_t^2 = \Delta_1^2 + \Delta_2^2 + \Delta_3^2$. The natural shape of the resonance (or the cross section curve of the resonance) is given by the Breit-Wigner single-level expression:

$$\sigma(E_r - E) = \frac{\sigma_0}{(E_r - E)^2 + \Gamma^2/4},$$

where E_r is the resonance energy, $(E_r - E)$ is the devia-

tion from resonance energy, and Γ is the full width at half-maximum. Assume that an incoming proton penetrates the target a distance x losing energy δE , before producing the (p, γ) interaction in the slab of target dx . The yield for the reaction from this slab of target from the segment of beam dE can be written

$$y(dE) = N_E(dE)n_0\sigma[E_r - (E - \delta E)],$$

where n_0 is the number of target nuclei per cm^2 and is assumed to be constant. The total yield from the element of beam dE at E can be found by integrating from $E = E$ to $E = 0$, or some number small enough so that the contribution from the low-energy side of the curve is very small. Since $\dot{E} = E$ at $x = 0$, and $E = 0$ at

TABLE VI. Parameters used for evaluating Eq. (8).

Reaction	E_r Mev	Input aperture	Δ_1 ev	Δ_2 ev	Δ_3 ev	Δ_t ev	Γ ev
$Al^{27}(p, \gamma)Si^{28}$	0.9924	0.010 in.	39	17	46	63	50, 100, 150
$C^{13}(p, \gamma)N^{14}$	1.7476	0.010 in.	69	30	87	115	25, 75, 125
$Ni^{58}(p, \gamma)Cu^{59}$	1.4241	0.030 in.	168	24	37	174	50, 100
$Ni^{58}(p, \gamma)Cu^{59}$	1.8437	0.030 in.	218	31	42	224	50, 100, 150

TABLE VII. Results of the present measurements of the full width at half-maximum of several (p,γ) resonances. Column 3—here Γ is determined by finding the $\frac{1}{4}$ - $\frac{3}{4}$ position on the rise of the thick-target yield curve. Column 4— Γ is determined by comparison of experimental data with theoretical shape.

Reaction	Energy Mev	Γ Interquartile	Γ	Other results and references	
$F^{19}(p,\alpha\gamma)O^{16}$	0.3405	2.4 ± 0.3 kev		3 ± 1 kev ^a	2.9 ± 0.2 kev ^b 3.3 ± 0.2 kev ^c
$F^{19}(p,\alpha\gamma)O^{16}$	0.4836	0.9 ± 0.1 kev		2.2 ± 0.2 kev ^b	
$F^{19}(p,\alpha\gamma)O^{16}$	0.8724	4.5 ± 0.3 kev		4.5 ± 0.2 kev ^c	5.4 ± 0.3 kev ^d
$Al^{27}(p,\gamma)Si^{28}$	0.9924		100 ± 50 ev	60 ± 30 ev ^e	100 ev ^f
$C^{13}(p,\gamma)N^{14}$	1.7476		75 ± 50 ev	2.1 ± 0.2 kev ^g	< 400 ev ^h
$Ni^{58}(p,\gamma)Cu^{59}$	1.4241		50 ± 50 ev		
$Ni^{58}(p,\gamma)Cu^{59}$	1.8436		100 ± 50 ev		

^a See reference 26.

^b See reference 28.

^c See reference 16.

^d See S. E. Hunt and K. Firth, Phys. Rev. **99**, 786 (1955).

^e See H. H. Staub, Nuovo cimento **6**, 306 (1957).

^f Bender, Shoemaker, Kaufmann, and Bourcius, Phys. Rev. **76**, 273 (1949).

^g J. D. Seagrave, Phys. Rev. **85**, 197 (1952).

^h See reference 22.

x = some very large number, δE can be replaced by kx and integration is from zero to infinity, where k is the constant energy loss through the target³¹:

$$y(dE) = N_E(dE)n_0 \int_0^\infty \frac{\sigma_0 k dx}{[E_r - (E - kx)]^2 + \Gamma^2/4}$$

To find the total yield, integrate the above over the energy distribution $N_E(dE)$:

$$y_{\text{(tot)}} = n_0 \int_0^\infty \frac{N_0}{(2\pi)^{1/2} \Delta_t} \exp\left[-\frac{(E_0 - E)^2}{2\Delta_t^2}\right] \times \left[\int_0^\infty \frac{\sigma_0 k dx}{[E_r - (E - kx)]^2 + \Gamma^2/4} \right] dE. \quad (8)$$

This equation can be evaluated numerically for the proper value of Δ_t obtaining a family of curves for various Γ 's. By normalizing the experimental results and comparing with these curves it is possible to obtain a value for Γ . Thick-target yield curves are shown in Fig. 12 for Al, C, and Ni (p,γ) resonances. The solid lines are the calculated curves for various Γ 's; the experimental points are indicated. Table VI is a summary of the parameters used in evaluating Eq. (8). The

³¹ The assumption of a constant energy loss per unit distance, equal to k , also involves the assumption that the incremental energy loss is very small relative to the width of the resonance so that the statistical processes of energy loss theory will apply. For a resonance of 100 ev width there may be some doubt in the validity of this assumption.

widths and the assigned errors, presented in Table VII, have been chosen by inspection of the curves.³²

IX. ACKNOWLEDGMENTS

We would like to acknowledge the competent assistance of the following individuals from the Naval Research Laboratory: Mr. J. F. Reynolds, Mr. J. Duncan, Mr. J. Rowe, Mr. R. Dunphy, Mr. Leo Schade (deceased), Mr. F. Koerber, and Mr. J. Borthwick of the Engineering Services Division; Dr. R. Belsheim and Mr. J. Bachman for assistance on strain gage measurements; Mr. B. Stennett and Mr. E. LeBeau of the Engineering Services Division shops for the final machining of the plates; Mr. R. D. Lee for help on vacuum problems; Dr. J. W. Butler, Nucleonics Division, for help with the mass-1 and mass-2 measurements; Dr. R. Drachman and Mrs. L. Shapiro, Nucleonics Division, for assistance with the calculations of the theoretical shapes of yield curves; and Mr. K. L. Dunning, Nucleonics Division, for constant support and many helpful discussions. The following individuals from the Naval Gun Factory are also due thanks for their aid: Mr. L. C. Garver and Mr. J. C. Gamble, Industrial Control Division; Mr. J. B. Clawson, Mr. F. N. Kidwell, and Mr. R. A. Schulze, Production Department; Mr. Kerzulis and Mr. Haynes, machinists.

³² Choosing Γ by inspection is justified first because the present data were taken primarily for energy calibration and second because of the relatively large number of unproven assumptions involved in the derivation of the expression, Eq. (8), giving the theoretical yield curve.